SCIENTIFIC REPORTS

OPEN

TiO_2 decorated functionalized halloysite nanotubes (TiO_2@HNTs) and photocatalytic PVC membranes synthesis, characterization and its application in water treatment

Received: 1 May 2018
Accepted: 22 February 2019
Published online: 13 March 2019

Gourav Mishra & Mausumi Mukhopadhyay

In this study photocatalyst, TiO_2@HNTs were prepared by synthesizing TiO_2 nanoparticles *in situ* on the functionalized halloysite nanotubes (HNTs) surface. Photocatalytic PVC membrane TiO_2@HNTs M2 (2 wt.%) and TiO_2@HNTs M3 (3 wt.%) were also prepared. Photocatalyst TiO_2@HNTs and photocatalytic PVC membranes were used to study the photocatalytic activity against the methylene blue (MB) and rhodamine B (RB) dyes in UV batch reactor. The structure and morphology of photocatalyst and photocatalytic PVC membrane were characterized by fourier transform infrared spectroscopy (FT-IR), X-ray diffraction (XRD), scanning electron microscopy (SEM), energy dispersive X-ray (EDX), transmission electron microscopy (TEM), UV-Vis spectrophotometer and photoluminescence (PL). The PL study showed that the oxygen vacancies and surface hydroxyl groups present on the surface of TiO_2@HNTs act as excellent traps for charge carrier, reducing the electron-hole recombination rate.TiO_2@HNTs 2 (2 wt.%) and TiO_2@HNTs 3 (3 wt.%) degraded MB dye up to 83.21%, 87.47% and RB dye up to 96.84% and 96.87%, respectively. TiO_2@HNT photocatalyst proved to be stable during the three consecutive cycle of photocatalytic degradation of the RB dye. TiO_2@HNTs M2 and TiO_2@HNTs M3 degraded MB dye up to 27.19%, 42.37% and RB dye up to 30.78%, 32.76%, respectively. Photocatalytic degradation of both the dyes followed the first-order kinetic model. Degradation product analysis was done using the liquid chromatography–mass spectrometry (LC-MS) and the results showed that the dye degradation was initiated by demethylation of the molecule. MB and RB dye degradation reaction were tested by TBA and IPA as OH^* and H^+ scavengers respectively. Mechanism of photocatalytic activity of TiO_2@HNTs and photocatalytic PVC membrane were also explained.

In recent years, halloysite nanotubes (HNTs) and its composite materials have attracted enormous attention due to their wide range of potential applications in fields of catalysis[1], adsorption[2], composites[3] and drug delivery processes[4] etc. Various materials like HNTs, carbon nanotubes (CNTs), graphene oxide (GO), silica, cerium oxide[5] and clay particles have been attached to photocatalysts[1] to improve the photocatalytic reactions. Amongst them, HNTs ($Al_2Si_2O_5(OH)_4{\cdot}2H_2O$) is a promising material due to its efficient physicochemical property and stability which has been tested in various studies[6–9]. HNTs are naturally occurring, eco-friendly alumino-silicate clay minerals with tube-like structure, consisting of two-layered aluminosilicate clay mineral with one alumina octahedron sheet and one silica tetrahedron sheet in 1:1 stoichiometric ratio[10,11]. They are suitable for the development of photocatalyst supported materials as they enable proper distribution of composite in suspensions. The presence of HNTs improves the synergistic effects and light absorption properties of photocatalyst supported materials. Hydroxyl groups found on its surface helps in better dispersion of HNTs in different solvents[12]. Comparatively, HNTs are more efficient than carbon nanotubes (CNTs) due to many –OH groups present on its surface and

Department of Chemical Engineering, Sardar Vallabhbhai National Institute of Technology Surat, Gujarat, India. Correspondence and requests for materials should be addressed to M.M. (email: mausumi_mukhopadhyay@yahoo.com or mmu@ched.svnit.ac.in)

different outside and inside chemical properties. The fact that HNTs are structurally similar to CNTs but cheaper than CNTs makes them ideal for research in photocatalysis and adsorption.

Photocatalysts are semiconductor that converts light energy into chemical energy of electron-hole pairs. An efficient photocatalyst must possess chemical and physical stability, must be cheap and nontoxic in nature[13]. Several semiconductor materials such as TiO_2, titanate nanosheets[14], cobalt hydroxide-amino complex[15], ZnO[16], CdS, g-C_3N_4 and Ag_3PO_4, and their nanostructure assemblies have been extensively employed as photocatalysts[17].

TiO_2 (nano range) has been greatly used in photocatalytic applications due to its exceptional properties such as quantum confinement and high surface to volume ratio[18–20]. Nano range TiO_2 powders have large specific areas and thus provide ample active sites for reaction to occur and enhance the catalytic activity. TiO_2 nanoparticles are prone to agglomerate which results in a decrease in the photocatalytic activity. Therefore, significant efforts have been made to minimize the agglomeration of TiO_2 nanoparticles, such as the use of supported methods, coating technology and so on[21].

HNTs as a support can also be used for nanoparticles synthesis to avoid their agglomeration[11,22–24]. TiO_2 with HNTs provides large specific surface area and also due to the mesoporous structure of HNTs, they may be potentially used as adsorbents, catalysts and catalyst support[25–27]. They have also been used to efficiently remove the organic pollutants by photocatalytic degradation in aqueous dispersions[28,29]. TiO_2 is widely used as a suitable semiconductor for treating oil spills and decomposing organic pollutants present in water and air[30–33]. Lvov and co-workers have extensively worked with HNTs and examined its properties by modifying it with silver nanorods, Ru, Rh, Pt, Co, Fe and copper-Nickel alloy nanoparticles to analyse the antimicrobial activity and photocatalytic activity of modified HNTs[11,34,35]. Papoulis *et al.* used anatase form of TiO_2 on palygorskite and halloysite surfaces to photocatalytical decompose NOx gas under visible-light and UV light irradiation[36]. Du, Y. and P. Zheng calcinated the TiO_2-HNT composite samples at different temperature and for TiO_2-HNT calcined at 300 °C, 81.6% MB is degraded after UV irradiation treatment for 4 h[37].

In another research, a one-step solvothermal method was used by Wang *et al.* for the preparation of TiO_2/HNTs samples for wastewater purification[21]. Zheng *et al.* fabricated an amylose–HNT–TiO_2 composite for effective removal of methylene blue (MB) and persistent organic pollutant 4-nitrophenol (4-NP) under UV irradiation[38]. Peng H. *et al.* fabricated the ZnO-HNTs photocatalyst and observed that ZnO bonded HNTs showed higher photocatalytic performance toward photo-degradation of MB dye[9]. However, it is complicated to separate nano-sized photocatalyst from treated water, and the possible toxic health effects associated with it[39], hence restricting its practical application.

In some studies, nano-sized TiO_2 is immobilized or dispersed onto various materials like glass[40], polymer[41,42] and clay[43]. In our previous work, we have synthesized TiO_2 nanoparticles on the surface of HNTs nanocomposite via the sol-gel method and blended it in different weight percentage (1–3 wt.%) of poly(vinyl chloride) (PVC) for the preparation of hybrid ultrafiltration membranes. The new hybrid membranes had improved permeation performance and enhanced antibacterial activity against *E. coli*.[44]. Damodar *et al.* also observed that almost 100% of *E. coli* is eradicated by 4% TiO_2/PVDF membrane after 1 min of UV irradiation[45]. Wittmer *et al.* prepared cellulose based TiO_2 photocatalyst to treat wastewater which acts as a precursor for the preparation of catalytically active membrane. However, after the regeneration of cellulose, a partial decrease in the catalytic activity is observed[46]. Zhang *et al.* studied the rejection of Direct Black 168 by using a TiO_2/Al_2O_3 composite membrane under UV irradiation at different pH of the wastewater. They observed that 82% of the Direct Black 168 is degraded due to TiO_2/Al_2O_3 composite membrane under UV irradiation after 300 min[47].

In this study, the HNTs surface is functionalized by using organosilane ((3-Aminopropyl)triethoxysilane)) as a coupling agent so that the HNTs surface becomes suitable for TiO_2 attachment. As the raw HNTs are less adhesive in nature, there is a risk of leaching out of TiO_2 during the course of the experiment. Thus the raw HNTs functionalized with organosilane coupling agent for proper attachment between TiO_2 and HNTs. After functionalization of HNTs, TiO_2 nanoparticles are synthesized on the surface of HNTs (TiO_2@HNTs) with the help of titanium (IV) isopropoxide (TIP) and ethanol solution. Novel photocatalytic PVC membranes are prepared by blending the TiO_2@HNTs photocatalyst in two different concentration i.e. 2 wt.% and 3 wt.% using a non-solvent phase induced method. The main aim for fabricating the TiO_2@HNTs photocatalyst and photocatalyst membrane is to exploit the photocatalytic activity of functionalized HNTs while avoiding the aggregation of TiO_2 nanoparticles and simultaneously reducing the electron-holes recombination rate of TiO_2 surface, thus improving the photocatalytic activity.

The structure and morphology of TiO_2@HNTs photocatalyst and photocatalytic PVC membrane are characterized by fourier transform infrared spectroscopy (FT-IR), X-ray diffraction (XRD), scanning electron microscopy (SEM), energy dispersive X-ray (EDX), transmission electron microscopy (TEM), UV-Vis spectrophotometer and photoluminescence (PL). The photocatalytic activity of TiO_2@HNTs photocatalyst (TiO_2@HNTs) alone and photocatalytic PVC membranes (TiO_2@HNTs M2 and TiO_2@HNTs M3) are investigated by using methylene blue (MB) and rhodamine B (RB) dyes degradation test. After MB and RB dye degradation test, end products are identified by a liquid chromatography–mass spectrometry (LC-MS).

Result and Discussions

Characterization of TiO_2@HNTs and photocatalytic PVC membranes. FT-IR spectra as shown in Fig. 1(a), confirmed the presence of functionalized HNTs after modification. When raw HNTs[48] were compared with the TiO_2@HNTs, some new FTIR peaks were observed in the spectrum like stretching CH_2 vibration band around 2934 cm^{-1}, and the deformation CH_2 and Si-CH vibration at 1627 cm^{-1} and1507 cm^{-1} respectively. Apart from these peaks, broad peak of O-H stretching of water at 3433 cm^{-1} was also seen. These observations confirmed the presence of silane coupling agent[49]. Silane coupling agent is used because its main function is to ensure proper bonding between TiO_2 and HNTs[49–52]. If this functionalization is not done, due to the absence of chemical conjugation[53], the TiO_2 may leach out during the course of the experiment because of the less adhesive nature of

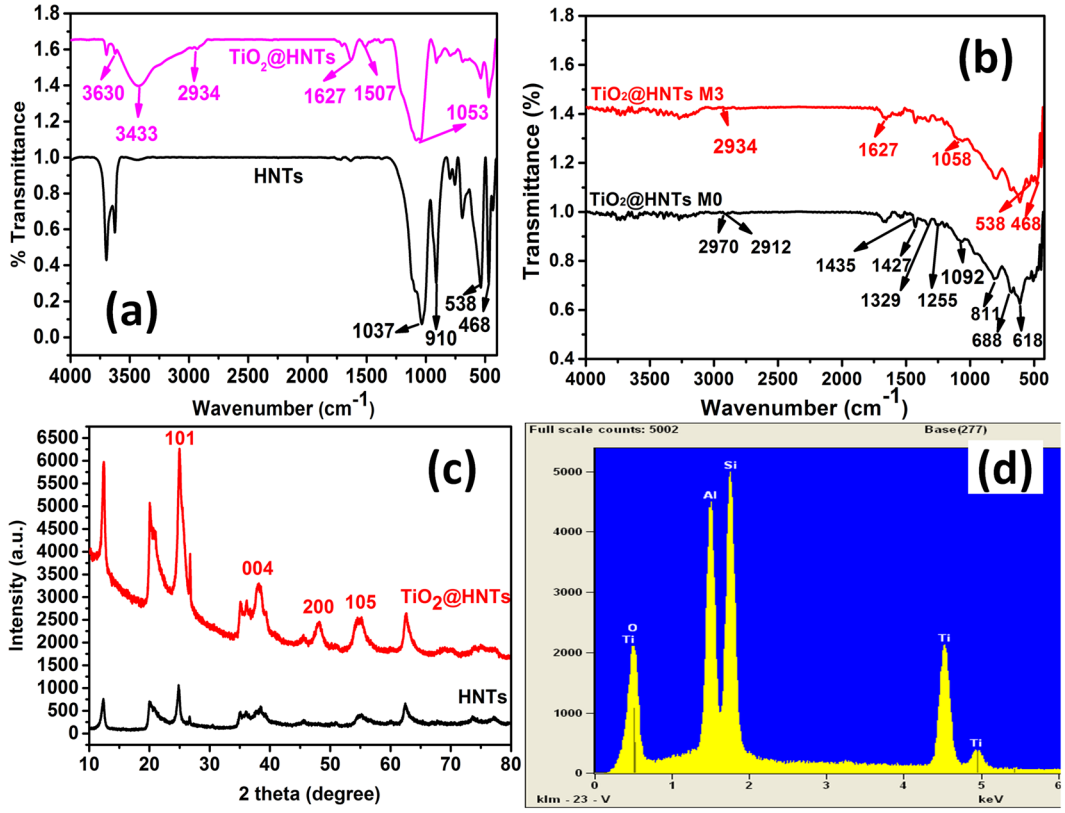

Figure 1. FT-IR spectra of raw HNTs and TiO_2@HNTs (**a**), raw PVC membrane (TiO_2@HNTs M0) and photocatalytic PVC membrane (TiO_2@HNTs M3) (**b**), XRD peaks of HNTs and TiO_2@HNTs (**c**) and (**d**) EDX spectra of TiO_2@HNTs photocatalyst.

raw HNTs[54,55]. The TiO_2@HNTs possess some significant signals, like distortions of aluminium-oxygen-silicon and silicon-oxygen-silicon bonds at 538 and 468 cm^{-1} respectively; and -OH groups of the inner hydroxyl groups at 909 cm^{-1}. Furthermore, for comparison, the broad stretching band of silicon-oxygen at about 1037 cm^{-1} shifts to about 1058 cm^{-1}, indicating hydrogen bonding between TiO_2 and HNTs[21]. In Fig. 1(b), ATR-FT-IR spectra of TiO_2@HNTs M0 and TiO_2@HNTs M3 with the principle bands of PVC were depicted. FT-IR spectrum of PVC reflects expected distinctive absorptions: 2970–2912 cm^{-1} attributed to stretching C-H of CHCl and stretching C-H of CH_2 group, 1435 cm^{-1} and 1427 cm^{-1} attributed to deformation wagging of CH_2 group, and 1331–1255 cm^{-1} shows the stretching of the C-H of CHCl groups. Stretching C-C (1092 cm^{-1}), rocking CH_2 (811 cm^{-1}), stretching C-Cl attributed to 688 cm^{-1} and 618 cm^{-1} respectively[56]. In Fig. 1b, the peaks of photocatalyst PVC membrane in the ATR-FT-IR results resembles the characteristic peaks belonging to both TiO_2@HNTs M0 and TiO_2@HNTs M3. Other characteristic absorption peaks for TiO_2@HNTs in the spectrum of the membrane was not clearly identified because of the overlap with absorption peaks of PVC polymer or the IR beam might not be able to penetrate properly enough to get distinct peaks of HNTs[57] in FTIR spectra (Fig. 1b).

The results of XRD clearly shows the specific peaks as shown in Fig. 1(c) which compares the XRD results of HNTs and TiO_2@HNTs synthesized. The peaks depicted for HNT sample can be translated into the characteristic peaks of halloysite shown in Fig. 1(c). Two fresh peaks, however, can be noticed at $2\theta = 48°$ and 54.1° and a stronger peak at $2\theta = 25.3°$ alongside with decline in the halloysite peaks due to the sol-gel method. Based on JCPDS 21–1272, all peaks related to TiO_2 properties can be indexed to the (101), (004), (200) and (105) planes of TiO_2 structure[58,59]. This verifies the successful preparation of TiO_2@HNTs. Similar results of XRD pattern also described by the Ghanbari *et al.*, in their study for the fabrication of high-performance thin film nanocomposite membranes[60]. Furthermore, in the EDX spectrum (Fig. 1d) confirms the loading of TiO_2 nanoparticles on the surface of HNTs with 24.42 wt%. Intense peaks of Ti and oxygen at 0.5 eV were observed which confirmed the presence of TiO_2 nanoparticles on the surface of HNTs.

Thermal behaviour of TiO_2@HNTs and TiO_2@HNTs/PVC blends was investigated from room temperature to 600 °C temperature range. The temperature was raised at the rate of 10 °C/min (Fig. 2). The raw HNTs showed a weight loss between 50 °C and 150 °C, which may be due to reduction in adsorbed water molecules[61]; and structural dehydroxylation of structural Al–OH groups between 450–550 °C[62]. Decomposition of the (3-Aminopropyl) triethoxysilane causes an additional weight loss in TiO_2@HNTs between 250 °C and 425 °C when compared with the raw HNTs[63] suggesting that the thermal stability, as well as the purity of the nanotubes, was high. PVC membrane (TiO_2@HNTs M0–0 wt.%) and TiO_2@HNTs membranes (TiO_2@HNTs M2 and TiO_2@HNTs M3) showed a different behaviour. The weight loss of the sample (around 60%) was mainly between temperature range 220 °C to 300 °C. The rest of the sample was thermally decomposed at 500 °C as shown in Fig. 2

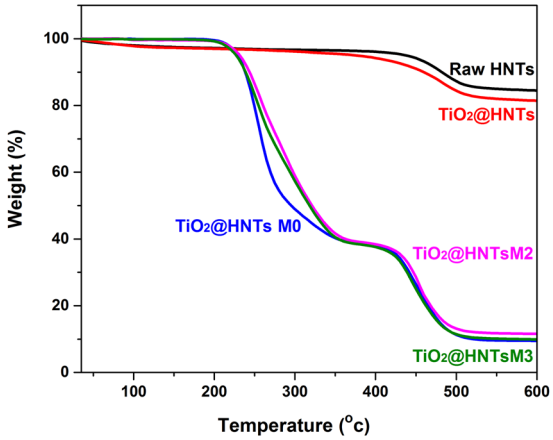

Figure 2. TGA curves of raw HNTs, TiO_2@HNTs and photocatalytic PVC membrane (TiO_2@HNTs M0-TiO_2@HNTs M3).

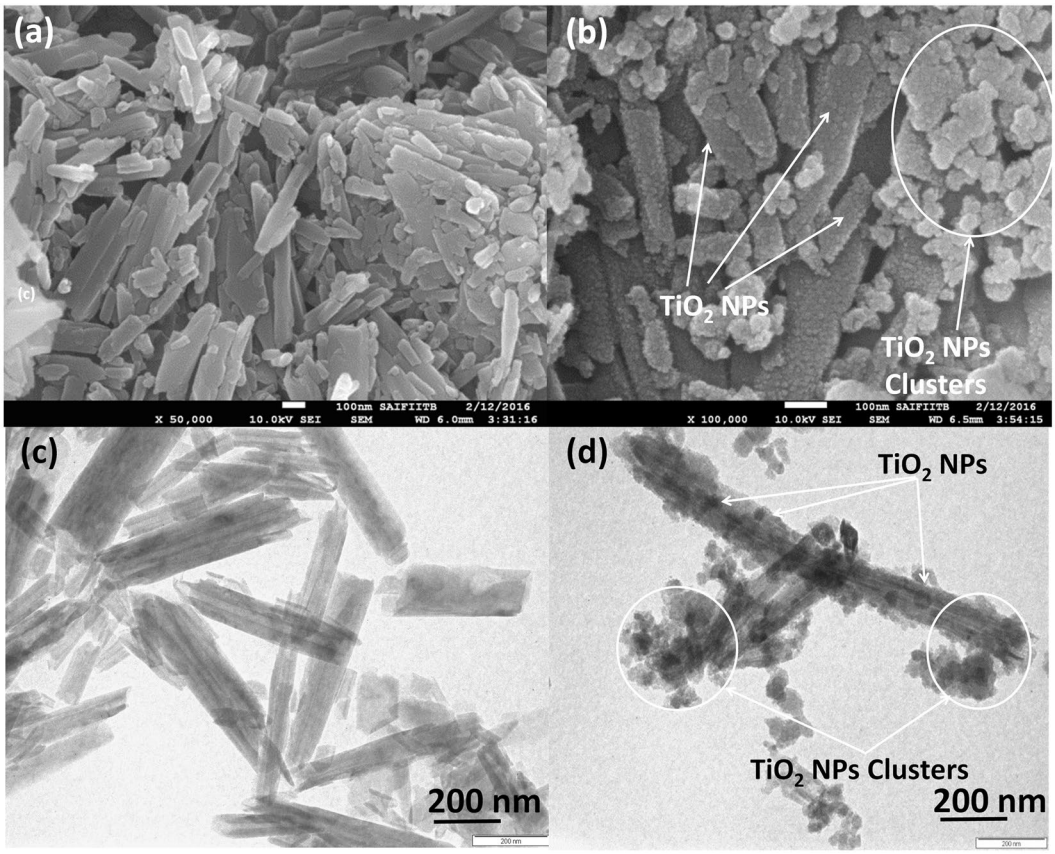

Figure 3. FEG-SEM of (**a**) raw HNTs, (**b**) TiO_2@HNTs and TEM images of (**c**) raw HNTs and (**d**)TiO_2@HNTs.

FEG-SEM and TEM were done to analyse the structural and morphological characteristics of raw HNTs and TiO_2@HNTs photocatalyst (Fig. 3). The TEM images of raw HNTs clearly show the hollow tubular structure with a diameter of 50–70 nm and length of 0.5–2 µm (Fig. 3c). The outer surface of HNTs was made up of silica and was surrounded by multi-walled aluminol layer. In Fig. 3b,d TiO_2 nanoparticles were seen to be randomly deposited on the surface of HNTs. Few aggregation or cluster of nanoparticles was observed in FEG-SEM and TEM analysis (Fig. 3b,d) which was formed when photocatalyst was separated from the solution during the fabrication process. The size of small particles and cluster size of this TiO_2 range from 10 nm to 80 nm. The presence of TiO_2 nanoparticles on the surface of HNTs confirms successful loading on HNTs.

All the membrane possessed typical asymmetric structure like that of ultrafiltration membranes and no distinct difference between the TiO_2@HNTs M0 (Fig. 4a) and the TiO_2@HNTs M2 and TiO_2@HNTs M3 (Fig. 4b,c)

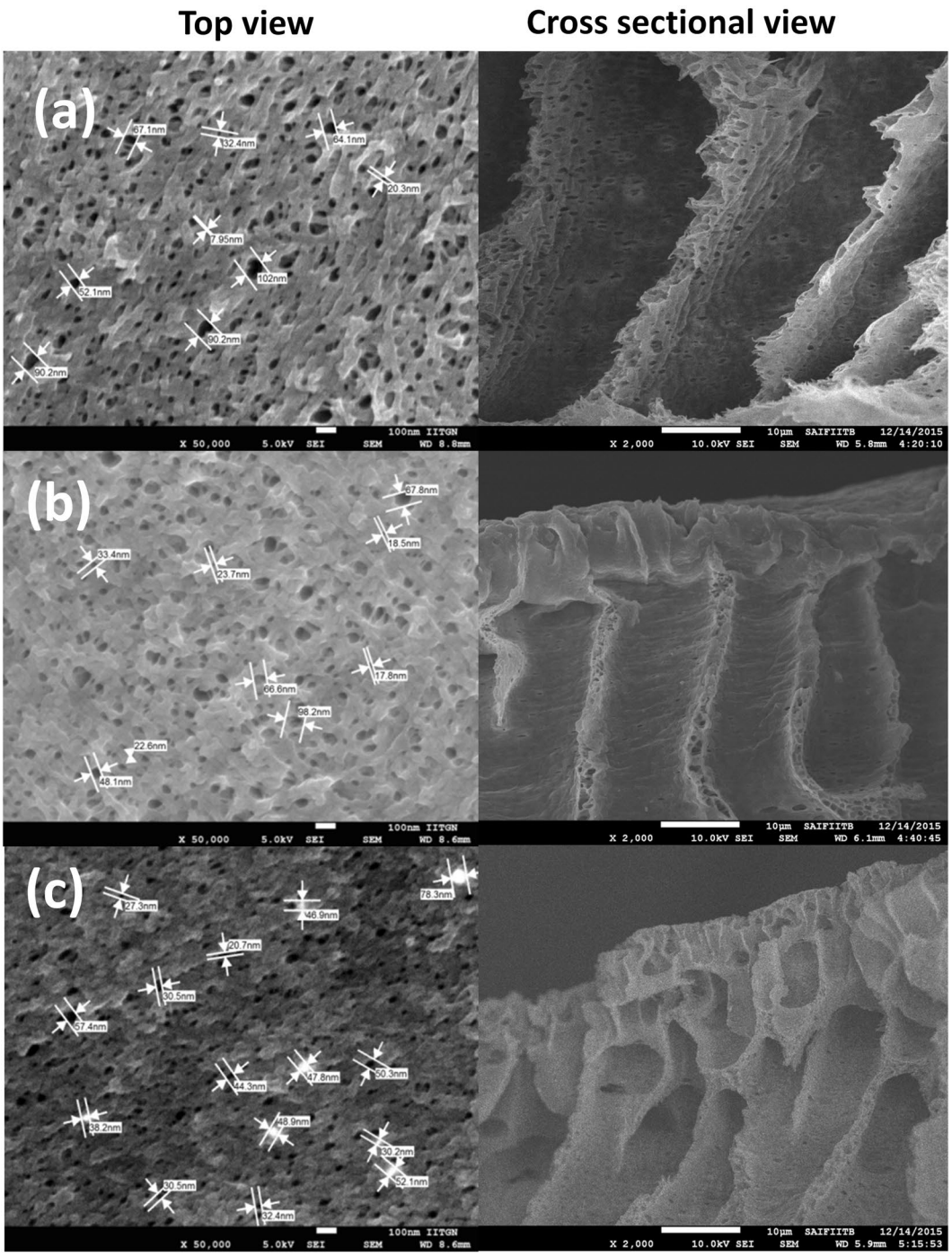

Figure 4. FEG-SEM images (top and cross-sectional view) of raw PVC membrane (**a**), and photocatalytic PVC membranes TiO_2@HNTs M2 (**b**) and TiO_2@HNTs M3 (**c**) samples.

on the top surface was observed. Only large pores were observed on the membrane surface as shown in Fig. 4(b,c) when compared with TiO_2@HNTs M0 (Fig. 4a). FEG-SEM images shows top surface and cross-sectional view of TiO_2@HNTs M0 and TiO_2@HNTs M2 and TiO_2@HNTs M3 membranes. All membrane samples were homogeneous and asymmetric in nature with macro-voids and finger-like structures formed because of the high mutual diffusivity of DMAc and water. This porous structure indicates that TiO_2@HNTs increases the membrane porosity without altering the membrane morphological structure[64].

To investigate the recombination of the free carrier in HNTs, photoluminescence (PL) emission spectrum was analysed. One broad PL peak centred under excitation of 450 nm visible light irradiation was observed in Fig. 5a. The broad-band at 624 nm indicates that the light for excitation can initiate electron transition from the valence band (VB) to the conduction band (CB) in HNTs. As a result of this transition, the electron/hole pair can be generated which then further recombine radiatively to give broad and strong PL signal under 450 nm

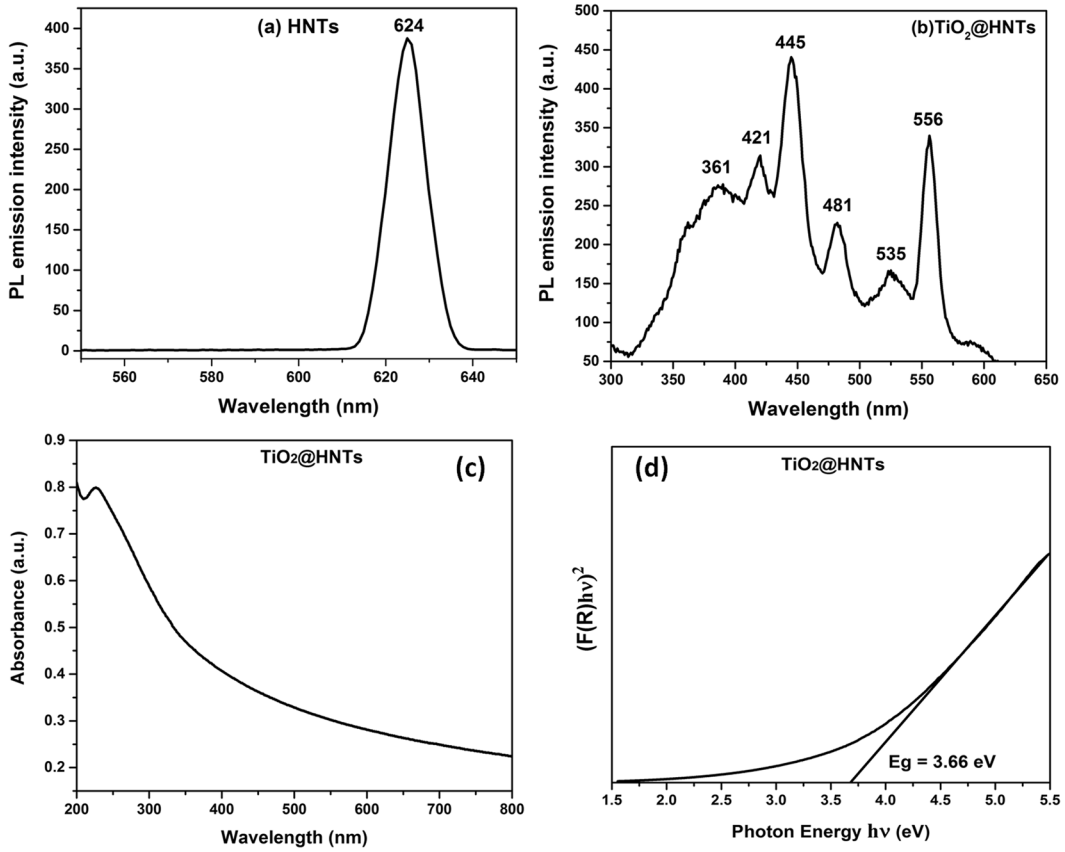

Figure 5. Photoluminescence (PL) emission spectra of (**a**) HNTs (**b**) TiO_2@HNTs (**c**) UV absorption spectra of TiO_2@HNTs and (**d**) band-gap energy spectra of TiO_2@HNTs.

light irradiation. The PL emission spectrum of TiO_2@HNTs was recorded at an excitation wavelength of 220 nm (high absorption region). The major peak at 361 nm (lower than the band edge emission) in PL emission spectra (Fig. 5b) was due to the band to band transition. At longer wavelengths in the visible region, the emission peaks at 421, 445, 481, 535 and 556 nm reflect the surface state emissions, located within the band gap of TiO_2@HNTs[65]. The oxygen vacancies and surface hydroxyl groups present on the surface of TiO_2 and HNTs acts as excellent traps for charge carrier, reducing the electron-hole recombination rate. Presence of oxygen vacancies from shallow trap state near the adsorption band edge act as efficient electron trap centres or colour centres. UV-Vis spectroscopy was used to study the light absorption properties. Figure 5c displays the UV-Vis absorption spectra of the prepared materials obtained. The band gap of pure TiO_2 is 3.2 eV and the absorption edge of the TiO_2@HNTs material is around 220 nm corresponding to the band gap energy (Eg) of 3.66 eV (Fig. 5d). This difference is due to the addition of HNTs because of which the modified photocatalyst gets excited to produce more electron-hole pairs under light irradiation, resulting in higher photocatalytic activity[66,67].

Photocatalytic activities of TiO_2@HNTs photocatalyst and photocatalytic PVC membranes for the degradation of MB and RB dye solutions. In Fig. 6 images of MB and RB dye degradation under 120 min of UV irradiation can be seen. Initially, the colour of MB dye solution was blue and RB dye solution was pink. After 120 min, the colour of TiO_2@HNTs 2 and 3 reaction mixture changed from blue to light blue in case of MB dye and from pink to colourless solution in case of RB dye.

This decolourization was due to degradation of dye and was highest in the case of TiO_2@HNTs 3. The chemical structure of MB and RB dye is shown in Fig. 7(a,b). To further confirm the degradation of dye, LC-MS chromatographic separation analysis was done. For the analysis, the dye solution was collected after 120 min of UV irradiation. As seen in Fig. 8(a–d), maximum absorption of MB dye in the visible region was at 664 nm and in the UV region two peaks located at 245 and 292 nm. The highest peak of MB dye at 664 nm is due to its centre benzene ring comprising sulphur and nitrogen whereas the two dimethylamine substituted aromatic ring exhibits its peak in the UV region at 245 and 292 nm. These high peaks at 664 nm gradually diminish with time in the presence of TiO_2@HNTs 3 under UV irradiation. Similarly, for RB dye, the characteristic absorption peak at 554 nm as shown in Fig. 9(a–d) also degrades with time. The $n \rightarrow \pi$ transition of C=N, C=O groups in the aromatic ring of the RB dye structure (Fig. 7b) is responsible for the colour of solution and its absorbance at 554 nm. During the reaction process, when the dye structure was disrupted by the TiO_2@HNTs 3 photocatalyst, the absorption intensity of RB dye decreased rapidly with change in colour from pink to a colourless solution.

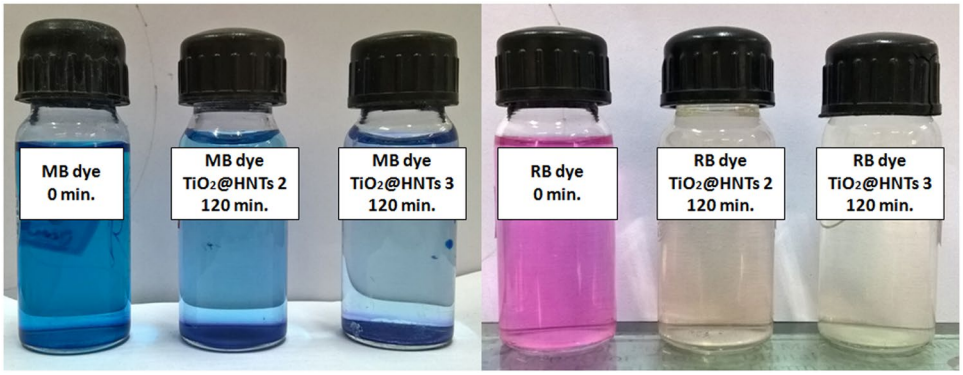

Figure 6. Digital photograph of MB and RB dyes under 120 min of UV irradiation.

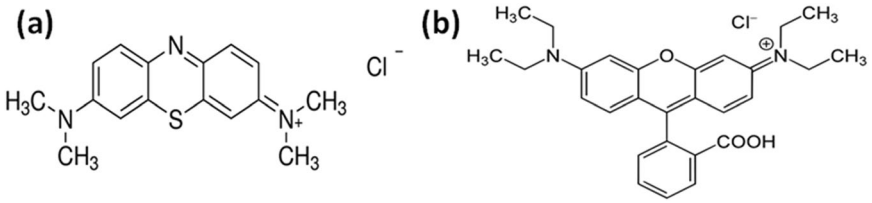

Figure 7. Structures of (**a**) methylene blue (MB) and (**b**) rhodamine B (RB) dyes.

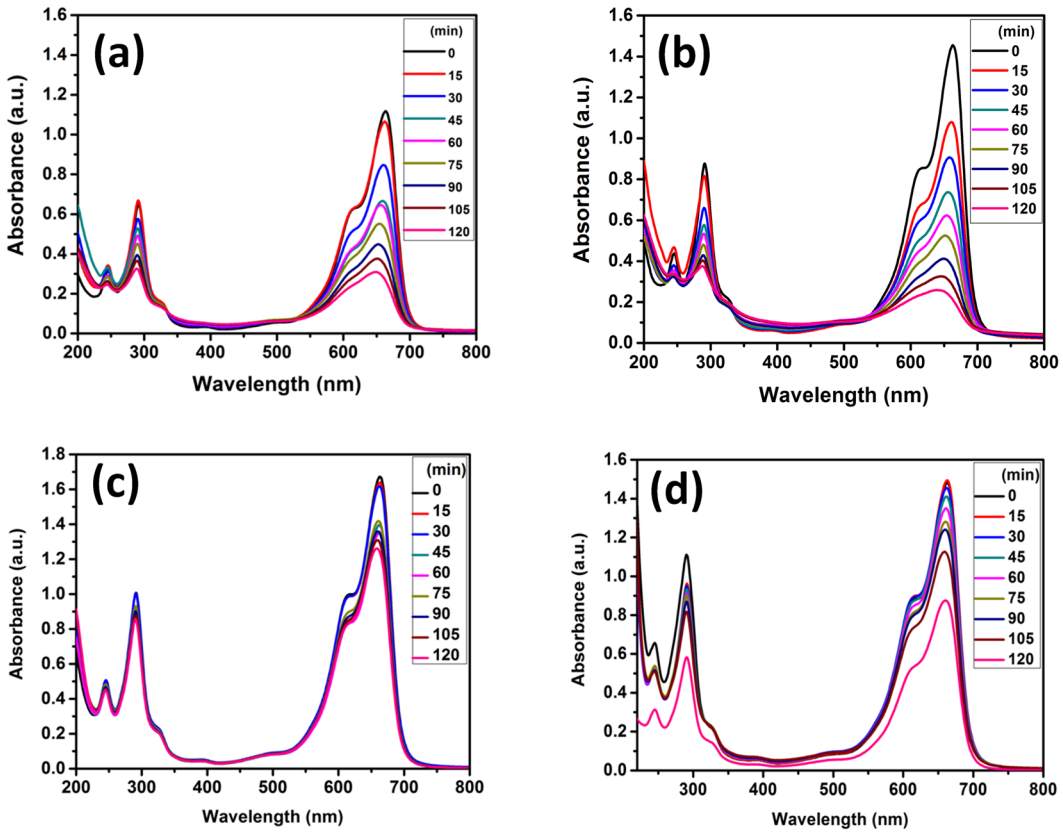

Figure 8. Photocatalytic degradation of MB dyes absorption spectra at different time intervals-TiO_2@HNTs 2 & 3 (**a**,**b**), photocatalytic PVC membranes TiO_2@HNTs M2 and TiO_2@HNTs M3 (**c**,**d**).

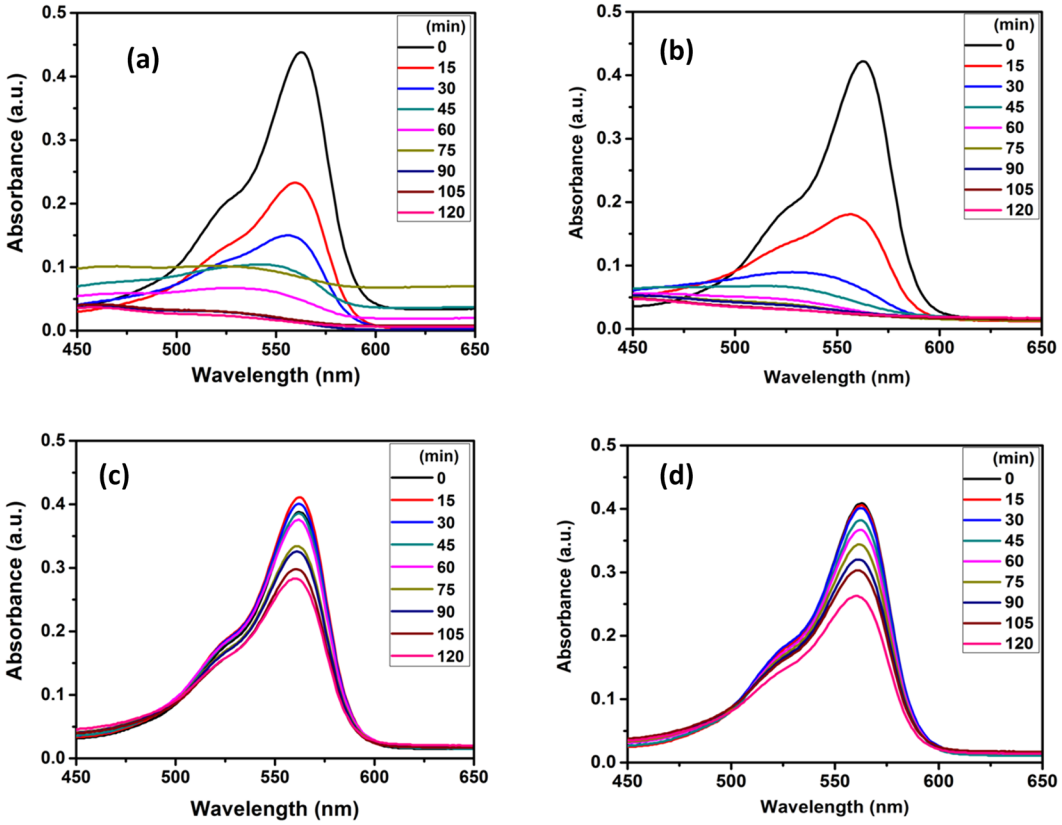

Figure 9. Photocatalytic degradation of RB dyes absorption spectra at different time intervals-TiO_2@HNTs 2 & 3 (**a**,**b**), photocatalyst PVC membrane TiO_2@HNTs M2 and TiO_2@HNTs M3 (**c**,**d**).

The shifts in the absorption spectra of both the dye solutions were studied during photocatalytic degradation analysis (Figs 8 and 9). The absorption peak of MB dye solution was at 664 nm which decreased gradually due to dye degradation and attained its lowest value at 120 min (Fig. 8a,b). The reason for the decrease in absorption peaks was attributed to the fact that TiO_2@HNTs photocatalyst cleaves the aromatic ring of the dye molecules and initiate its degradation[68]. In the case of RB dye solution, highest and characteristic peak was seen at 562 nm, which dipped quickly in the first 15 min of degradation and was lowest after 120 min (Fig. 9a,b). The MB dye was degraded up to 83.21% and 87.47% (Fig. 8a,b) for TiO_2@HNTs 2 and TiO_2@HNTs 3 respectively. In the case of RB dye, 2 wt.% of photocatalyst was sufficient enough for degradation of 20 mg/L of RB dye and the degradation rate for both the 2 wt.% and 3 wt.% photocatalyst was 96.84% and 96.87% (Fig. 9a,b) respectively. Blue Shift in absorption peaks (λ max) was observed gradually with time which finally resulted in the respective lowest absorption peak of dye. The adsorption capacity of prepared TiO_2@HNTs was also tested with MB and RB dye in dark condition at room temperature with 20 mg/L dye solution. The maximum dye adsorption efficiency of MB dye and RB dye were 17.5 mg/g and 4.8 mg/g for TiO_2@HNTs 2 and 12.10 mg/g and 3.67 mg/g for TiO_2@HNTs 3 respectively after 2 h. In the control experiment (HNTs 2 and HNTs 3), the removal of the MB dye was around 39.22% and 47.82% and RB dye was around 17.65% and 25.2% respectively after 2 h of irradiation. Also, there was a minor reduction in UV spectra even when TiO_2@HNTs photocatalyst was added and both MB and RB dye solution was kept in dark. Thus it was confirmed that the degradation was due to TiO_2 nanoparticles in the presence of UV irradiation.

Though photocatalytic PVC membranes TiO_2@HNTs M2 and TiO_2@HNTs M3 both exhibited photocatalytic activity (as shown in Figs 8c,d and 9c,d for MB and RB dyes respectively), but TiO_2@HNTs M3 membrane possessed more catalytic activity as compared to TiO_2@HNTs M2 because with the increase in the TiO_2@HNTs concentration the catalytic activity also enhances. However, it was observed that photocatalytic activity reduced in photocatalytic PVC membranes when compared with the same wt% of TiO_2@HNTs alone. The MB dye was degraded up to 27.19%, 42.37% (Fig. 8c,d) and RB upto 30.78%, 32.76% (Fig. 9c,d) for TiO_2@HNTs M2 and TiO_2@HNTs M3 respectively. The reason behind this slow rate of degradation in both TiO2@HNTs M2 and TiO2@HNTs M3 can be due to the reduction of active sites of TiO_2@HNTs photocatalyst during membrane preparation. During phase separation process, the increase in the amount of TiO_2@HNTs photocatalyst increases its catalytic activity but its increase after 3 wt.% in membrane casting solution may result in photocatalyst agglomeration[69]. This agglomeration hampers the number of free catalytic sites for dye degradation and also delays the phase separation process during membrane preparation[46]. When the concentration of photocatalyst increases in the solution, the turbidity of the solution increases and light is scattered more due to which screening effect occurs hampering the specific activity of the catalyst and reducing the degradation rate[70–72]. Thus an optimal

Samples	K [min^{-1}]	R^2
Methylene Blue		
HNTs 2	0.00182 ± 0.00006	**0.990**
TiO_2@HNTs 2	0.00605 ± 0.0002	**0.986**
TiO_2@HNTs M2	0.00117 ± 0.00005	**0.981**
HNTs 3	0.00197 ± 0.0001	**0.968**
TiO_2@HNTs 3	0.0073 ± 0.0002	**0.993**
TiO_2@HNTs M3	0.00193 ± 0.0001	**0.969**
Rhodamine B		
HNTs 2	0.00701 ± 0.00002	**0.989**
TiO_2@HNTs 2	**1st** 0.01675 ± 0.001 **2nd** 0.00745 ± 0.0005	**0.984** **0.983**
TiO_2@HNTs M2	0.00134 ± 0.00009	**0.959**
HNTs 3	0.00231 ± 0.0005	**0.996**
TiO_2@HNTs 3	**1st** 0.02258 ± 0.001 **2nd** 0.00236 ± 0.0002	**0.970** **0.964**
TiO_2@HNTs M3	0.00136 ± 0.00007	**0.976**

Table 1. Rate parameter of photo-catalytic activity of MB and RB dye.

amount of photocatalyst must be used for photocatalytic degradation process for increased degradation and reduced inaccuracy.

The kinetics of photocatalytic reactions can be described using the first-order reaction for concentrations (20 mg/L) of MB and RB dye solutions. The rate constants (k) and the correlation coefficient (R^2) has been evaluated using linear regression curve of $\ln(C_0/C)$ versus UV light irradiation time. First-order rate equations are as follows[73]:

$$\ln \frac{[C_0]}{[C]} = kt \tag{1}$$

Here, k is the first order rate constant (min^{-1}); [C] and [C_0] final and initial dye concentration in (mg/L), respectively.

The degradation efficiency has been calculated using[74]:

$$\text{Degradation}(\%) = \left(\frac{C_0 - C}{C_0}\right) \times 100 \tag{2}$$

where C_0 is the initial concentration of the dye and C is the concentration of the dyes after UV irradiation in the selected time interval.

The correlation coefficient (R^2) was calculated to be nearly as high as $R^2 \approx 0.95–0.99$ which reiterate the suitability of the first-order reaction listed in Table 1. MB and RB degradation rate are shown in Fig. 10c,d, where the TiO_2@HNTs photocatalyst has notably improved the photocatalytic activity. During photocatalysis of RB dye by TiO_2@HNTs 2 and 3, dye adsorption process occurred in two steps shown in Fig. 10d. At first stage, RB molecules diffuse from the aqueous solution to the external surface of TiO_2@HNTs or the boundary layer diffusion of RB molecules. Secondly, gradual adsorption occurred until equilibrium was reached. The linear portion of the first stage did not pass through the origin, indicating the existence of a boundary layer resistance between TiO_2@HNTs photocatalyst and dye solution[75] Similar observation is reported in literature[73]. Furthermore, the detailed photocatalytic mechanism is described in detail in a later section.

The stability of the TiO_2@HNTs photocatalyst was estimated by recycling the photocatalyst for degradation of RB dye under UV light irradiation for three times. The loss of the photocatalytic activity was negligible (approximately 6% after 3 repeated runs) (Fig. 11) which signifies the stability of TiO_2@HNTs photocatalyst in terms of its non photo-corrosive nature during the photocatalytic degradation of the model dye molecules, which proved to be very important for its practical applications.

Photocatalytic PVC membrane activity Test with MB dye. To evaluate the photocatalytic property of the membrane surface, control (raw PVC membrane TiO_2@HNTs M0), TiO_2@HNTs M2 and TiO_2@HNTs M3 samples were treated with UV light without stirring for 1 h (Fig. 12). After 1 h of irradiation TiO_2@HNTs M2 and TiO_2@HNTs M3, sample colour disappears from the membrane surface. On the contrary, the change in colour in control experiment was less after irradiation of UV light. The change in colour of membrane of the control sample was seen to be least when irradiated with UV light, which was contrary to the result of samples of TiO_2@HNTs M2 and TiO_2@HNTs M3. TiO_2 acts as a semiconductor and presence of UV light results in the formation of electrons and holes. These photo-generated electrons hence formed, reduces Ti (IV) cations to the Ti (III) state and the holes oxidise O_2^{-}* anions[76]. Simultaneously O_2 atoms are propelled out producing a set of O_2 vacancies on the surface. These vacancies were filled by water molecules present in the environment and adsorbed OH groups are formed on the surface, increasing the hydrophilicity of the surface[77]. Also, the radicals hence produced can degrade the dye molecules present around the membrane surface (detail mechanism explained in the mechanism

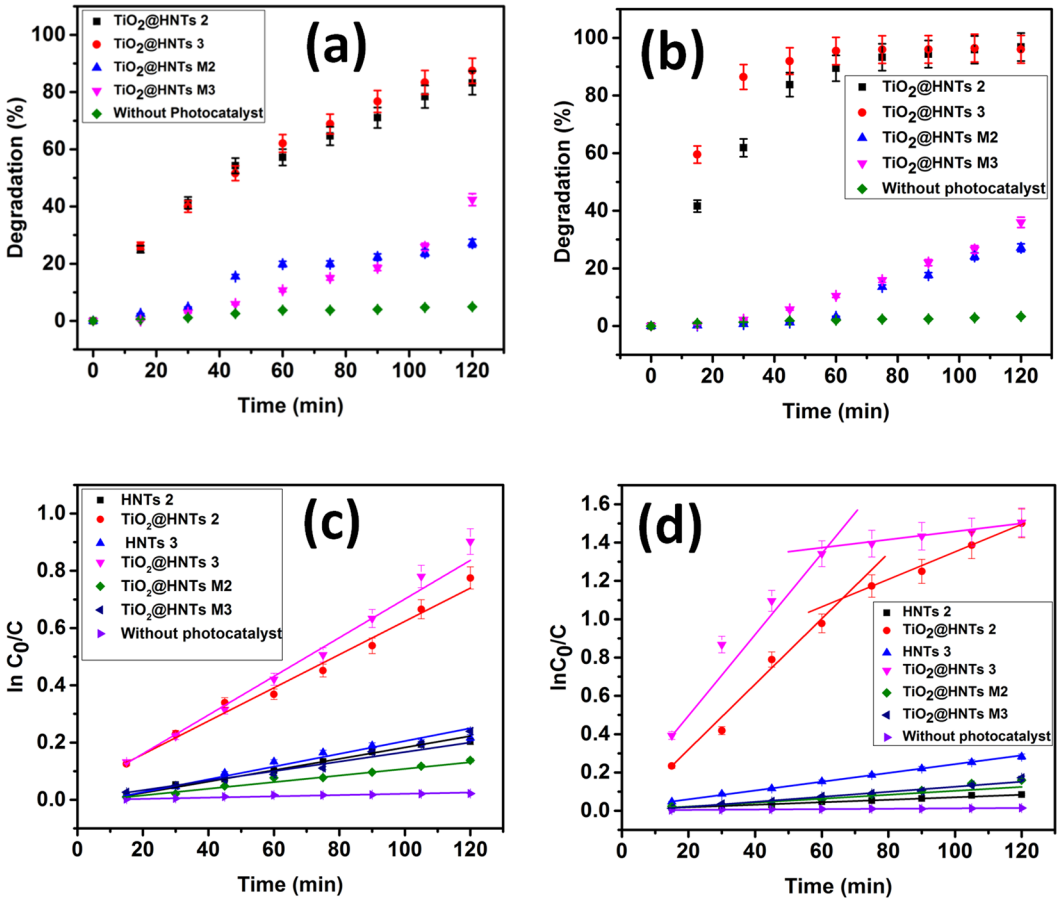

Figure 10. The percent rate of degradation of MB dye (**a**) and RB dye (**b**) and rate constant k for MB dye (**c**) and RB dye (**d**) for all samples.

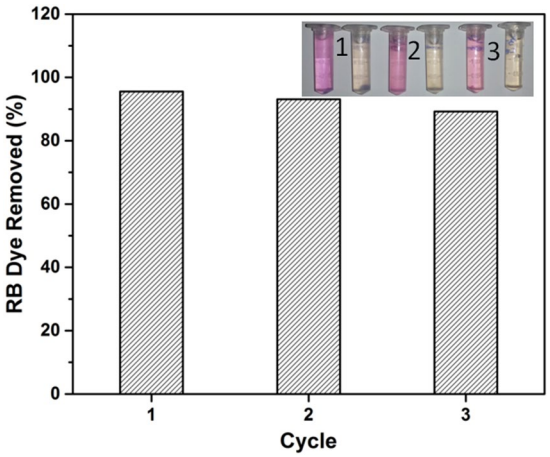

Figure 11. Photocatalytic stability test of TiO_2@HNTs photocatalyst.

section). For the reproducibility, a test procedure was repeated with five membrane pieces for each sample. MB dye showed better contrast while taking digital images and hence was preferred for photographic images.

Photocatalytic Mechanism of TiO_2@HNTs photocatalyst and Photocatalytic membrane. When irradiated with UV light, the HNTs do not get excited, rather it acts as an electrical insulator and hence any charge generated on TiO_2 surface during UV irradiation cannot be transferred to HNTs. These electrostatic attraction and repulsion forces contribute together for an efficient movement and separation of e^- and h^+ on TiO_2[1]. Apart from being a charge carrier separator, HNTs also enhance dye degradation. Due to the negatively charged surface of HNTs, the dye molecule (cationic in nature) are brought closer to the TiO_2, increasing the

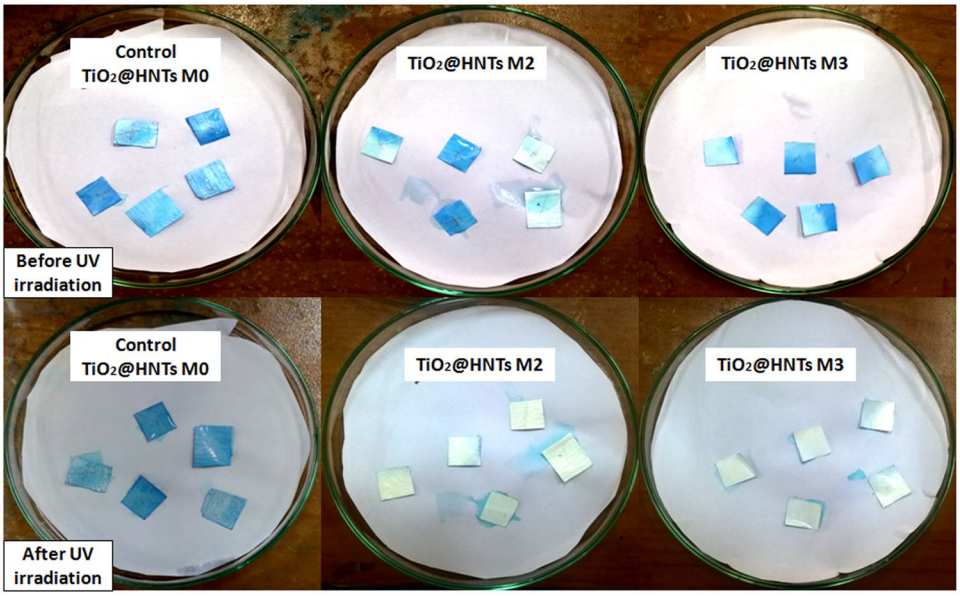

Figure 12. Photograph of photocatalytic PVC membrane TiO_2@HNTs M2 & TiO_2@HNTs M3 treated the sample with MB before and after 1 h of UV irradiation.

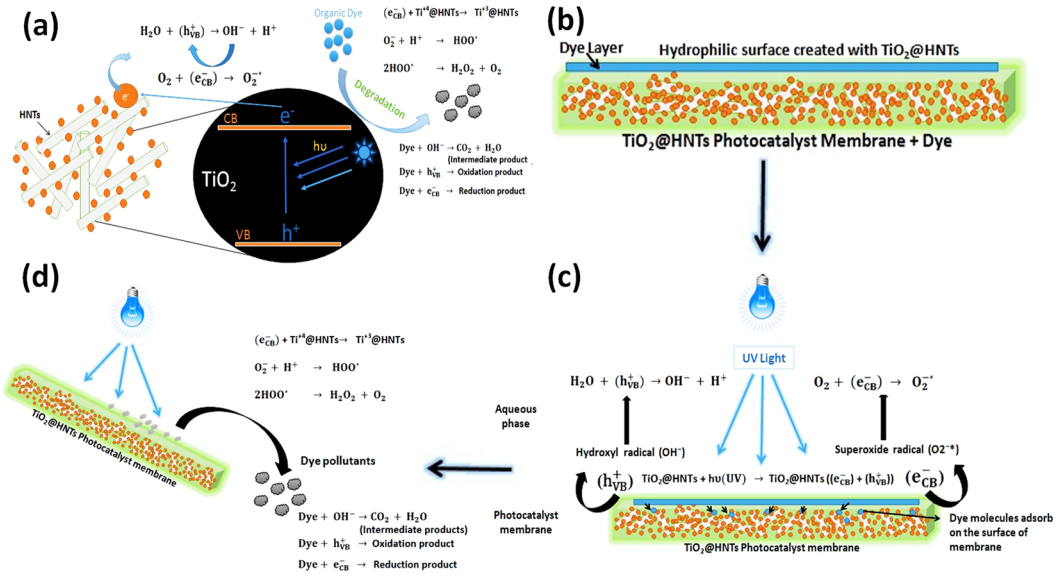

Figure 13. Schematic representation of the photocatalytic activity of TiO_2@HNTs photocatalyst (**a**) and photocatalytic membrane (**b** to **d**).

adsorption rate of the dye molecules. The detailed mechanism of the photocatalyst TiO_2@HNTs and photocatalyst membrane are shown in Fig. 13. When TiO_2@HNTs is irradiated by UV light, a photoelectron moves from valence band of TiO_2@HNTs to the empty conduction band. This photon has the energy ($h\upsilon$) equal to or greater than the band gap. Thus a hole is created in VB (h^+_{VB}) and an electron (e^-_{CB}) in CB generated as shown in Fig. 13(a). These (h^+_{VB}) then produce OH* radical after reacting with H_2O. Now, these OH* radicals act as a potent oxidising agent and oxidise adsorbed organic molecules which are in near vicinity of TiO_2@HNTs surface Fig. 13b. Simultaneously O_2 atoms are propelled out producing a set of O_2 vacancies on the surface. These vacancies are filled by water molecules present in the environment and results in the formation of adsorbed OH groups on the surface, increasing surface hydrophilicity[77]. These photo-generated electrons hence formed, reduces Ti^{+4}@HNTs cations to the Ti^{+3}@HNTs state and the holes oxidise O_2^{-}* anions. Also, the radicals hence produced can degrade the dye molecules present around the membrane surface as shown in Fig. 13c. The efficiency of the breakdown of these organic molecules depends upon their stability and structure. OH* radicals also degrade the pollutant present around it. The electrons in (e^-_{CB}) conduction band meanwhile reacts with O_2 and generate superoxide radicals (O_2^{-}*), which accelerates oxidation process (Fig. 13d) and also hinders any further e−/hole recombination

S. No.	Photocatalyst/Photocatalytic membrane	Method	Target	Performance	Time	Ref.
1	TiO_2@HNTs	Sol-gel method Phase inversion	RB and MB	TiO_2@HNTs degraded up to 87%, 96% and PVC photocatalytic membranes degraded up to 42.37%, 32.76% MB and RB respectively	2 h	**Present study**
2	TiO_2@HNTs	Sol-gel method	MB	MB dye degradation upto 81.6%	4 h	[37]
3	TiO_2@HNTs	Solvothermal method	Acetic acid Methanol	Degradation of acetic acid 3488.63 μmol/g and methanol 729.37 μmol/g	1–2 h	[21]
4	TiO_2 nanotube membranes	Through-hole morphology	RB	RB dye degradation up to 28%	5.3 h	[89]
5	TiO_2-Polyvinylidene fluoride	Plasma-induced graft polymerization	Reactive Black 5 dye	Removed 30–42% of 50 mg/L aqueous Reactive Black 5 dye	—	[90]
6	TiO_2-Al_2O_3 membrane	Sol-gel processing method	Methyl orange	Removed 27% of 5 mg/L aqueous methyl orange	9 h	[91]

Table 2. Studies of photocatalyst and photocatalyst membrane performance as reported in the literature.

formation, thus maintaining electron neutrality within the TiO_2 molecule. The H^+ formed in reaction further reacts with O_2^-* formed and protonates the hydroperoxyl radical (HO_2^-*). Hence finally hydroxyl radical (OH^*) is formed, which is highly reactive in nature.

To understand the role and the involvement of active species in degradation process, control experiments were performed using scavengers for the photo-generated holes and free radicals. Photo-degradation of MB and RB dyes were investigated in the presence of UV light with the TiO_2@HNTs photocatalyst to observe the role and the importance of degradation by free radicals. Isopropanol (IPA) and Tert-butyl alcohol (TBA) were used as H^+ and hydroxyl radical (OH*) scavenger respectively. In both reactions with MB and RB dye, H^+ showed no significant effect on photocatalytic degradation, while OH* free radical affected the MB and RB photocatalytic degradation reactions. Adding TBA (0.02 mmol) in the reaction, photocatalytic degradation decreased from 87.47% to 44% in case of MB dye while in case of RB dye degradation percentage decreases from 96.87% to 72%. This proved that OH* free radicals were generated during photodegradation of dye. Several researchers[78] have suggested that the OH* radical produced by the oxidation of water or OH^- radicals by holes at the surface, diffuses towards the solution to oxidise the organic compound. H_2O_2 and hydroxylated degradation products were formed during the reaction and the efficiency of degradation increases significantly when H_2O_2 is formed in the presence of UV radiation. This was because of free hydroxyl radicals (which act as powerful oxidizing agent) generated by the dissociation of H_2O_2 in the presence of UV irradiations. Moreover, a high concentration of hydroxyl peroxides itself acts as a scavenger which reduces the concentration of hydroxyl radicals and compound elimination efficiency. The generated hydroxyl radicals attack the MB and RB dye structure at different sites like un-saturation points etc. In several such attacks, the MB and RB dyes get converted into CO_2 and hetero-atoms which are further mineralized as mentioned in Supplementary File Tables S2 and S3. The combination of TiO_2@HNTs photocatalyst has both the advantages of being an efficient charge carrier separator and good absorbent for positively charged molecules[1]. The photocatalytic activity was also enhanced due to the absorptivity of HNTs and the crystalline TiO_2 nanoparticles which facilitate the interaction of dye and reactive TiO_2@HNTs photocatalyst. Also, the agglomeration of TiO_2 nanoparticles was avoided by the homogeneous dispersion of TiO_2 nanoparticles on the HNTs surface.

The experimental data confirm that after 120 min of UV irradiation, the dye solution gets degraded with the formation of intermediate and end products. A mass spectroscopic (MS) study of the dye solution was also done to determine the intermediate and end products which were formed due to the cleavage of aromatic rings during the dye degradation process and eluted out at different retention time as per their mass and suggested structures. The difference in the concentration and composition of the products lead to many peaks with different intensities. Mass spectra and the possible structures of the dye degradation products are listed in Supplementary Table S2 and Table S3 for MB and RB dye[79–81]. The demethylation cleavage has also been reported in the literature during the photocatalytic degradation[79,80,82–84].

For evaluation of the activity of a photocatalyst, commonly time dependence of the concentration loss of dye under UV irradiation is measured. However, there are many factors that govern the reaction rate and kinetics. These experimental conditions include the concentration of the photocatalyst, the surface area of the photocatalyst, the amount of the photocatalyst used in the experiment and the UV light intensity and more. Table 2 summarises some recently synthesized photocatalyst with their photocatalytic experimental data.

Conclusion

Utilization of naturally present HNTs as photocatalyst support is advantageous for the synthesis of TiO_2@HNTs photocatalyst nanoparticles due to its size and shape dependent photocatalytic properties. In this study, TiO_2@HNTs photocatalyst and photocatalytic PVC membranes are synthesized. The prepared photocatalyst is stable and exhibits enhanced photocatalytic activity for the degradation of MB and RB dye solution under UV irradiation. The photocatalytic PVC membrane also exhibits similar photocatalytic activity against MB and RB dye but the degradation is slower as compared to the TiO_2@HNTs photocatalyst of the same weight.

Due to the electrostatic interaction between TiO_2 and HNTs surface, the photocatalyst has more e^- and h^+ pairs resulting in high photocatalytic activity. In the case of MB and RB dye which are positively charged, HNTs improved the supply and stability of the photo-generated charges and enhanced the absorption capability of the dye molecule on the photocatalyst. This was because of electrostatic attractive and repulsion forces originating

S. No.	Photocatalyst/photocatalytic membrane (with abbreviation)	Photocatalyst (g)	PVC (g)	PVP (g)	DMAc (g)
1.	TiO_2@HNTs 2 (2 wt%)	0.056	—	—	—
2.	TiO_2@HNTs 3 (3 wt%)	0.084	—	—	—
3.	TiO_2@HNTs M0 (0 wt%)	0.00	2.80	0.2	17
4.	TiO_2@HNTs M2 (2 wt%)	0.056	2.74	0.2	17
5.	TiO_2@HNTs M3 (3 wt%)	0.084	2.71	0.2	17

Table 3. Photocatalyst amount and composition of photocatalytic PVC membrane (for 20 ml) casting solution.

from the negatively charged HNTs surface. The stability of the TiO_2@HNTs photocatalyst is non photo-corrosive nature during the three consecutive cycle of photocatalytic degradation of the model dye molecules, which is very important for its practical applications. The MB and RB degradation catalysed by a TiO_2@HNTs and photocatalyst PVC membrane followed the first-order kinetic model. Therefore, the capabilities of nano range TiO_2@HNTs photocatalyst to degrade dyes may be exploited for wastewater purification in various textile and chemical industries.

Materials and Methods

Materials. HNTs, Titanium (IV) isopropoxide(TTIP) and Poly (vinyl chloride) polymer were furnished by Sigma-Aldrich. (3-Aminopropyl)triethoxysilane (silane coupling agent) was purchased from Himedia. Tert-butyl alcohol (TBA) (99%) and isopropanol (IPA) (99%) were purchased from s-d Fine Chem. Ltd, Mumbai. Rhodamine B (RB) and Methylene blue (MB) dyes were provided by Colourtex Pvt. Ltd., Surat, Gujarat. All other chemicals were also of analytical grade and were used without any purification. The water used was Elix millipore pure water (DI).

TiO_2@HNTs photocatalyst preparation. For the preparation of photocatalyst, moisture was removed from the inner/outer surfaces of raw HNTs by drying them for 4 h at 400 °C. 30 ml of silane coupling agent was mixed with 100 ml of toluene and 10 g of dried HNTs was then added into the silane-toluene solution to make it functional[53]. The mixture was then stirred at 125 °C for 18 h. After this, the mixture of functionalized HNTs was centrifuged and then washed with isopropanol (3–4 times). Vacuum drying chamber was further used for drying of the pellet at 60 °C. To synthesize TiO_2 nanoparticles on functionalized HNTs surface, 1 g of silane HNTs was mixed with titanium (IV) isopropoxide (TIP) - ethanol solution (ratio 1:15) by dispersing it into the deionised water (pH value adjusted by adding HNO_3 or NH_4OH). This solution was then vigorously stirred for sol-gel preparation. Hydrolysis reaction was initiated when TIP solution interacted with water molecules making the solution turbid and resulting in the increase of temperature to 60–70 °C for 18–20 h. When the peptization process was complete, stirring was stopped and centrifugation was done to retrieve TiO_2@HNTs mixture, which was then subjected to vacuum drying chamber overnight at 65 °C[85,86]. At last, the calcination of TiO_2@HNTs was done by heating it in a muffle furnace for 2 h (400 °C)[44].

Photocatalytic PVC membranes. The photocatalytic PVC membranes were prepared based on the principle of classical phase inversion method. The mixture containing TiO_2@HNTs photocatalyst (2 wt.% and 3 wt.% by weight of PVC) and DMAc solvent (85 wt.% by weight of the solution) was stirred at 600 rpm for 1 h to get the photocatalyst dispersed properly in the solvent. For the formation of pores, PVP (1 wt.% by weight of the solution) and PVC (14 wt.% by weight of the solution) polymer were added into the mixture (shown in Table 3). For uniform dispersion, the mixture was vigorously stirred for 12 h. After stirring, a homogeneous casting solution thus obtained was then degassed (room temperature) and poured on a glass slide with the help of membrane applicator (thickness 150 µm). The glass plate was then dipped immediately in a pure water bath for 12 h (room temperature) for the proper phase inversion process. Two photocatalytic PVC membranes (Table S4) were prepared based on the weight% of TiO_2@HNTs photocatalyst added in the membrane casting solution.

Characterizations. *Fourier transform-infrared (FT-IR) spectroscopy.* 3000 Hyperion Microscope with Vertex 80 FTIR System (Bruker, Germany) was used for the characterization of raw HNTs, TiO_2@HNTs and photocatalytic membrane. Scan range was 450–4500 cm^{-1}.

Thermo-gravimetric analysis (TGA). Samples were heated from room temperature to 600 °C at the rate of 10 °C min^{-1} under flowing nitrogen using a Diamond TG/DTA (Perkin Elmer, USA) instrument.

X-ray diffraction (XRD). HNTs and TiO_2@HNTs Photocatalyst powder samples were put into the sample collector for X-ray diffraction analysis with PANalytical, The Netherlands, scan rate 2 degrees/min. XRD peaks were recorded in the reflection mode in the angular range of 10–80° with (2 theta) angle.

Transmission electron microscopy (TEM). The morphological characteristics of raw HNT and TiO_2@HNTs were studied by a CM 200 transmission electron microscope (Philips). The samples were dispersed in deionized water, and then the suspended particles were transferred to a copper grid.

Field emission gun-scanning electron microscopes (FEG-SEM) with EDS. JSM-7600F FEG-SEM was used for determination of the structure of raw HNT and TiO_2@HNTs which had an energy dispersive X-ray spectrum (EDS, Inca Energy-200) at an accelerating voltage of 200 kV.

Photoluminescence spectra. At room temperature, the photoluminescence spectra were recorded with a Cary Eclipse fluorospectrometer using 220 and 450 nm Ar^+ laser as excitation source.

Band gap energy. For determining the absorption coefficient, optical energy gap (Eg) and nature of transitions involved, the optical absorbance spectra of TiO_2@HNTs (at room temperature) were studied. The thickness of the quartz cuvette (t), the optical absorption coefficient (α) was determined from the measurement of wavelength (λ). Generally,the absorption coefficient (α) was related to photon energy ($h\nu$) by known equation[87,88]:

$$(\alpha h\nu) = \beta(h\nu - E_g)^n$$

where, β signifies a constant known as band tailing parameter, Eg: energy of the optical band gap and n: power of the transition.

To convert the absorption spectra, in place of α, the kubelka-Munk function was used to eliminate any tailing contribution from UV spectra. The following function was applied to convert the absorption spectra:

$$F(R) = \frac{(1 - R)^2}{2R}$$

where R, the reflectance E_g values were estimated from plot of $(F(R)\, h\nu)^2$ *versus* energy by extrapolating the linear part.

Liquid chromatography–mass spectrometry (LC-MS). The chromatographic experiments with LCMS system were carried out on an Agilent 1290 Infinity UHPLC System, 1260 infinity Nano HPLC with Chipcube, 6550 iFunnel Q-TOFs (Agilent Technologies, USA) with a Column, binary pump and an autosampler. Acetonitrile was used as mobile phase solvent. The mass spectrometer was equipped with an electrospray ionization (ESI) source. The mass range was from 50 to 1000 *m/z*. Degradation products were monitored by LC-MS. Measurement conditions are listed in Supplementary Table S1.

Methods. *Photo-catalytic reaction experiments.* The possible photocatalytic activities of the TiO_2@HNTs 2, TiO_2@HNTs 3, TiO_2@HNTs M2 and TiO_2@HNTs M3 membranes were examined by assessing the MB and RB dye degradation which was prepared in an aqueous medium. UV batch reactor was used to carry out the photocatalytic reaction at a low pressure of 125 W UV lamp (254 nm) and Photon flux (Φ) = 1.69×10^{20} s^{-1} m^{-2} with continuous stirring. The photoreactor was initially filled with 100 mL of a 20 mg/L aqueous dye solution along with different weight percentage of a photocatalyst for the process and also with a different weight percentage of photocatalytic PVC membranes. The different concentration and combination used in the reactorare mentioned below. A UV−visible spectrophotometer (HACH, DR 6000, USA) was used to record the absorption magnitude of the dye solution regularly and similar steps was performed for both the dyes, after regular time intervals, at wavelengths of 664 nm for MB and 562 nm for RB dye respectively. Similarly, the photocatalytic efficiency of photocatalytic PVC membranes (TiO_2@HNTs M2 and TiO_2@HNTs M3) were also assessed. Initially, the membranes were dried and cut into small pieces and then dispersed into the aqueous dye solution for 1 h under constant stirring, after which dye solution irradiated with UV light, the concentration was analysed by a UV−visible spectrophotometer at regular intervals.

For comparative analysis, two different weight percentage of TiO_2@HNTs photocatalyst (accordingly photocatalyst added in membrane casting solution) and photocatalytic PVC membranes were used for this study under following conditions –

(i) MB and RB dye solution exposed to UV light in the absence of HNTs, TiO_2@HNTs photocatalyst and photocatalytic PVC membrane (adsorption of dyes).
(ii) MB and RB dye solution irradiated with UV light with only HNTs. (denoted as HNTs 2 and HNTs 3 i.e 2 wt.% and 3 wt.%)
(iii) MB and RB dye solution were irradiated with UV light with only TiO_2@HNTs photocatalyst (denoted as TiO_2@HNTs 2 and TiO_2@HNTs 3, a similar weight of photocatalyst added in membrane casting solution). In addition, we have also taken a higher concentration of photocatalyst in the reaction.
(iv) MB and RB dye solution irradiated with UV light with photocatalytic PVC membranes (denoted as TiO_2@HNTs M2 and TiO_2@HNTs M3 i.e 2 wt.% and 3 wt.% photocatalyst added in membrane casting solution as mentioned in membrane preparation section)
(v) Scavenger effects on the MB and RB dye degradation reaction were also tested by using TBA and IPA (with 0.2 mmol solutions) as hydroxyl radical (OH^*) and H^+ scavengers respectively.

Batch mode adsorption experiments. Adsorption experiments were performed containing 2 wt.% and 3 wt.% of TiO_2@HNTs photocatalyst and dye solution (20 mg/L MB and RB). The conical flasks were placed on a magnetic stirrer for 2 h. MB and RB dye concentrations in the solution were analyzed by UV-Vis spectrophotometer at different time intervals during the reaction. The amount of dye on TiO_2@HNTs photocatalyst adsorb was calculated from the following equation

$$q_e = \frac{(c_i - c_f) \times V}{M}$$

where, q_e (mg/g): the amount of dye adsorbed, C_i and C_f (mg/L): the concentrations of dye at initial and equilibrium respectively, V (L): the volume of the solution and M (g): the mass of dry TiO_2@HNTs photocatalyst used.

Photocatalytic PVC membrane activity test with MB dye. Photocatalytic PVC membrane TiO_2@HNTs M2 and TiO_2@HNTs M3 pieces (1 cm^2 per piece) with control membrane were dipped into 20 ml aqueous dye solution of MB dye and kept in dark for1 h. Membrane pieces were then positioned in open petri dishes individually and kept in UV light (Philips 15 W UV light). Digital images of these membranes were captured after keeping them on petri plates in dark and after exposure to UV light.

References

1. Christoforidis, K. *et al*. Solar and visible light photocatalytic enhancement of halloysite nanotubes/gC 3 N 4 heteroarchitectures. *RSC Advances* **6**, 86617–86626 (2016).
2. Cavallaro, G., Lazzara, G., Milioto, S., Parisi, F. & Sanzillo, V. Modified halloysite nanotubes: nanoarchitectures for enhancing the capture of oils from vapor and liquid phases. *Applied Materials & Interfaces* **6**, 606–612 (2013).
3. Amjadi, M., Samadi, A. & Manzoori, J. L. A composite prepared from halloysite nanotubes and magnetite (Fe3O4) as a new magnetic sorbent for the preconcentration of cadmium(II) prior to its determination by flame atomic absorption spectrometry. *Microchimica Acta* **182**, 1627–1633, https://doi.org/10.1007/s00604-015-1491-y (2015).
4. Sun, P. *et al*. Effective activation of halloysite nanotubes by piranha solution for amine modification via silane coupling chemistry. *RSC Advances* **5**, 52916–52925 (2015).
5. Lakhotia, S. R., Mukhopadhyay, M. & Kumari, P. Cerium oxide nanoparticles embedded thin-film nanocomposite nanofiltration membrane for water treatment. *Scientific reports* **8**, 4976 (2018).
6. Zhai, R. *et al*. Immobilization of enzyme biocatalyst on natural halloysite nanotubes. *Catalysis Communications* **12**, 259–263 (2010).
7. Zhang, Y., Ouyang, J. & Yang, H. Metal oxide nanoparticles deposited onto carbon-coated halloysite nanotubes. *Applied Clay Science* **95**, 252–259 (2014).
8. Lvov, Y. M., Shchukin, D. G., Mohwald, H. & Price, R. R. Halloysite clay nanotubes for controlled release of protective agents. *ACS nano* **2**, 814–820 (2008).
9. Peng, H., Liu, X., Tang, W. & Ma, R. Facile synthesis and characterization of ZnO nanoparticles grown on halloysite nanotubes for enhanced photocatalytic properties. *Scientific reports* **7**, 2250 (2017).
10. Ballav, N., Choi, H. J., Mishra, S. B. & Maity, A. Polypyrrole-coated halloysite nanotube clay nanocomposite: synthesis, characterization and Cr (VI) adsorption behaviour. *Applied Clay Science* **102**, 60–70 (2014).
11. Vinokurov, V. A. *et al*. Formation of metal clusters in halloysite clay nanotubes. *Science and Technology of advanced MaTerialS* **18**, 147–151 (2017).
12. Zhang, Y., Tang, A., Yang, H. & Ouyang, J. Applications and interfaces of halloysite nanocomposites. *Applied Clay Science* **119**, 8–17 (2016).
13. Molinari, R., Caruso, A. & Palmisano, L. In *Comprehensive Membrane Science and Engineering* (eds Enrico Drioli & Lidietta Giorno) 165–193 (Elsevier, 2010).
14. Soontornchaiyakul, W., Fujimura, T. & Sasai, R. Photocatalytic Oxidative Decomposition of Methylene Blue by Rh-Doped Titanate Nanosheets ([Ti4− x Rh x O9] 2−). *Bulletin of the Chemical Society of Japan* **90**, 1267–1272 (2017).
15. Walsh, D., Sanchez-Ballester, N. M., Ting, V. P., Ariga, K. & Weller, M. T. Visible light promoted photocatalytic water oxidation: proton and electron collection via a reversible redox dye mediator. *Catalysis Science &. Technology* **6**, 3718–3722 (2016).
16. Maeda, K. & Domen, K. Development of novel photocatalyst and cocatalyst materials for water splitting under visible light. *Bulletin of the Chemical Society of Japan* **89**, 627–648 (2016).
17. Wen, J., Xie, J., Chen, X. & Li, X. A review on g-C3N4-based photocatalysts. *Applied surface science* **391**, 72–123 (2017).
18. Lakhotia, S. R., Mukhopadhyay, M. & Kumari, P. Surface-modified nanocomposite membranes. *Separation & Purification Reviews*, 1–18 (2017).
19. Yu, J., Liu, W. & Yu, H. A one-pot approach to hierarchically nanoporous titania hollow microspheres with high photocatalytic activity. *Crystal growth and design* **8**, 930–934 (2008).
20. Nguyen-Phan, T.-D., Kim, E. J., Hahn, S. H., Kim, W.-J. & Shin, E. W. Synthesis of hierarchical rose bridal bouquet-and humming-top-like TiO_2 nanostructures and their shape-dependent degradation efficiency of dye. *Journal of colloid and interface science* **356**, 138–144 (2011).
21. Wang, R. *et al*. Photocatalytic activity of heterostructures based on TiO_2 and halloysite nanotubes. *ACS applied materials & interfaces* **3**, 4154–4158 (2011).
22. Jiang, G., Lin, Z., Zhu, L., Ding, Y. & Tang, H. Preparation and photoelectrocatalytic properties of titania/carbon nanotube composite films. *Carbon* **48**, 3369–3375 (2010).
23. Wang, S., Wang, T., Chen, W. & Hori, T. Phase-selectivity photocatalysis: a new approach in organic pollutants' photodecomposition by nanovoid core (TiO2)/shell (SiO2) nanoparticles. *Chemical Communications*, 3756–3758 (2008).
24. Zou, W., Zhang, J. & Chen, F. Preparation, characterization and application of TiO 2 nanoparticles surface-modified by DDAT. *Materials Letters* **64**, 1710–1712 (2010).
25. Occelli, M. L. New routes to the preparation of pillared montmorillonite catalysts. *Journal of Molecular Catalysis* **35**, 377–389 (1986).
26. Sterte, J. Synthesis and properties of titanium oxide cross-linked montmorillonite. *Clays and Clay Minerals* **34**, 658–664 (1986).
27. Ménesi, J. *et al*. Photocatalytic oxidation of organic pollutants on titania–clay composites. *Chemosphere* **70**, 538–542 (2008).
28. Kibanova, D., Trejo, M., Destaillats, H. & Cervini-Silva, J. Synthesis of hectorite–TiO2 and kaolinite–TiO2 nanocomposites with photocatalytic activity for the degradation of model air pollutants. *Applied Clay Science* **42**, 563–568 (2009).
29. Mogyorósi, K., Farkas, A., Dékány, I., Ilisz, I. & Dombi, A. TiO_2-based photocatalytic degradation of 2-chlorophenol adsorbed on hydrophobic clay. *Environmental science & technology* **36**, 3618–3624 (2002).
30. Nishimoto, S.-I., Ohtani, B., Kajiwara, H. & Kagiya, T. Correlation of the crystal structure of titanium dioxide prepared from titanium tetra-2-propoxide with the photocatalytic activity for redox reactions in aqueous propan-2-ol and silver salt solutions. *Journal of the Chemical Society, Faraday Transactions 1: Physical Chemistry in Condensed Phases* **81**, 61–68 (1985).
31. Hoffmann, M. R., Martin, S. T., Choi, W. & Bahnemann, D. W. Environmental applications of semiconductor photocatalysis. *Chemical reviews* **95**, 69–96 (1995).
32. Martí, M., Fetter, G., Domí, J., Melo-Banda, J. & Ramos-Gomez, R. Catalytic hydrotreating of heavy vacuum gas oil on Al-and Ti-pillared clays prepared by conventional and microwave irradiation methods. *Microporous and Mesoporous Materials* **58**, 73–80 (2003).
33. El-Kemary, M., Abdel-Moneam, Y., Madkour, M. & El-Mehasseb, I. Enhanced photocatalytic degradation of Safranin-O by heterogeneous nanoparticles for environmental applications. *Journal of Luminescence* **131**, 570–576 (2011).

34. Sanchez-Ballester, N. M. *et al*. Activated interiors of clay nanotubes for agglomeration-tolerant automotive exhaust remediation. *Journal of Materials Chemistry A* **3**, 6614–6619 (2015).
35. Abdullayev, E. *et al*. Natural tubule clay template synthesis of silver nanorods for antibacterial composite coating. *ACS applied materials & interfaces* **3**, 4040–4046 (2011).
36. Papoulis, D. *et al*. Palygorskite-and halloysite-TiO2 nanocomposites: synthesis and photocatalytic activity. *Applied Clay Science* **50**, 118–124 (2010).
37. Du, Y. & Zheng, P. Adsorption and photodegradation of methylene blue on TiO_2-halloysite adsorbents. *Korean Journal of Chemical Engineering* **31**, 2051–2056 (2014).
38. Zheng, P., Du, Y., Chang, P. R. & Ma, X. Amylose–halloysite–TiO2 composites: preparation, characterization and photodegradation. *Applied surface science* **329**, 256–261 (2015).
39. Gwinn, M. R. & Vallyathan, V. Nanoparticles: health effects—pros and cons. *Environmental health perspectives* **114**, 1818 (2006).
40. Hofstadler, K., Bauer, R., Novalic, S. & Heisler, G. New reactor design for photocatalytic wastewater treatment with TiO_2 immobilized on fused-silica glass fibers: photomineralization of 4-chlorophenol. *Environmental science &. technology* **28**, 670–674, https://doi.org/10.1021/es00053a021 (1994).
41. Dhananjeyan, M. R. *et al*. Photodynamics and surface characterization of TiO_2 and Fe_2O_3 photocatalysts immobilized on modified polyethylene films. *The Journal of Physical Chemistry B* **105**, 12046–12055, https://doi.org/10.1021/jp011339q (2001).
42. Uchida, H. *et al*. Preparation and properties of size-quantized TiO_2 particles immobilized in poly(vinylpyrrolidinone) gel films. *Langmuir* **11**, 3725–3729, https://doi.org/10.1021/la00010a023 (1995).
43. Thiruvenkatachari, R., Ouk Kwon, T. & Shik Moon, I. Application of Slurry Type Photocatalytic Oxidation-Submerged Hollow Fiber Microfiltration Hybrid System for the Degradation of Bisphenol A (BPA). *Separation Science and Technology* **40**, 2871–2888, https://doi.org/10.1080/01496390500333160 (2005).
44. Mishra, G. & Mukhopadhyay, M. Flux improvement, rejection, surface energy and antibacterial properties of synthesized TiO2-Mo. HNTs/PVC nanocomposite ultrafiltration membranes. *New Journal of Chemistry* **41**, 15049–15057 (2017).
45. Damodar, R. A., You, S.-J. & Chou, H.-H. Study the self cleaning, antibacterial and photocatalytic properties of TiO2 entrapped PVDF membranes. *Journal of Hazardous Materials* **172**, 1321–1328, https://doi.org/10.1016/j.jhazmat.2009.07.139 (2009).
46. Wittmar, A., Vorat, D. & Ulbricht, M. Two step and one step preparation of porous nanocomposite cellulose membranes doped with TiO_2. *RSC Advances* **5**, 88070–88078, https://doi.org/10.1039/c5ra16337d (2015).
47. Zhang, H., Quan, X., Chen, S., Zhao, H. & Zhao, Y. Fabrication of photocatalytic membrane and evaluation its efficiency in removal of organic pollutants from water. *Separation and purification technology* **50**, 147–155, https://doi.org/10.1016/j.seppur.2005.11.018 (2006).
48. Wang, L., Chen, J., Ge, L., Zhu, Z. & Rudolph, V. Halloysite-nanotube-supported Ru nanoparticles for ammonia catalytic decomposition to produce CO x-free hydrogen. *Energy & Fuels* **25**, 3408–3416 (2011).
49. Yuan, P. *et al*. Functionalization of halloysite clay nanotubes by grafting with γ-aminopropyltriethoxysilane. *The Journal of Physical Chemistry C* **112**, 15742–15751 (2008).
50. Datta, K., Achari, A. & Eswaramoorthy, M. Aminoclay: a functional layered material with multifaceted applications. *Journal of Materials Chemistry A* **1**, 6707–6718 (2013).
51. Li, C., Fu, L., Ouyang, J. & Yang, H. Enhanced performance and interfacial investigation of mineral-based composite phase change materials for thermal energy storage. *Scientific reports* **3**, 1908 (2013).
52. Yang, H., Li, M., Fu, L., Tang, A. & Mann, S. Controlled assembly of Sb 2 S 3 nanoparticles on silica/polymer nanotubes: insights into the nature of hybrid interfaces. *Scientific reports* **3**, 1336 (2013).
53. Zhang, Y., He, X., Ouyang, J. & Yang, H. Palladium nanoparticles deposited on silanized halloysite nanotubes: synthesis, characterization and enhanced catalytic property. *Scientific reports* **3** (2013).
54. Zhang, Y. & Yang, H. Halloysite nanotubes coated with magnetic nanoparticles. *Applied Clay Science* **56**, 97–102 (2012).
55. Wang, L., Chen, J., Ge, L., Rudolph, V. & Zhu, Z. Halloysite nanotube supported Ru nanocatalysts synthesized by the inclusion of preformed Ru nanoparticles for preferential oxidation of CO in H2-rich atmosphere. *The Journal of Physical Chemistry C* **117**, 4141–4151 (2013).
56. Turhan, Y., Dogan, M. & Alkan, M. Poly (vinyl chloride)/kaolinite nanocomposites: characterization and thermal and optical properties. *Industrial & Engineering Chemistry Research* **49**, 1503–1513 (2010).
57. Mishra, G. & Mukhopadhyay, M. Enhanced antifouling performance of halloysite nanotubes (HNTs) blended poly(vinyl chloride) (PVC/HNTs) ultrafiltration membranes: For water treatment. *Journal of Industrial and Engineering Chemistry* **63**, 366–379 (2018).
58. Abdel-Monem, Y. K. Efficient nanophotocatalyt of hydrothermally synthesized Anatase TiO 2 nanoparticles from its analogue metal coordinated precursor. *Journal of Materials Science: Materials in Electronics* **27**, 5723–5728 (2016).
59. Bumajdad, A., Madkour, M., Abdel-Moneam, Y. & El-Kemary, M. Nanostructured mesoporous Au/TiO2 for photocatalytic degradation of a textile dye: the effect of size similarity of the deposited Au with that of TiO2 pores. *Journal of Materials Science* **49**, 1743–1754 (2014).
60. Ghanbari, M. *et al*. Super hydrophilic TiO2/HNT nanocomposites as a new approach for fabrication of high performance thin film nanocomposite membranes for FO application. *Desalination* **371**, 104–114, https://doi.org/10.1016/j.desal.2015.06.007 (2015).
61. Yao, W. *et al*. Synthesis and characterization of high efficiency and stable Ag3PO4/TiO2 visible light photocatalyst for the degradation of methylene blue and rhodamine B solutions. *Journal of Materials Chemistry* **22**, 4050–4055, https://doi.org/10.1039/c2jm14410g (2012).
62. Chen, Y., Zhang, Y., Liu, J., Zhang, H. & Wang, K. Preparation and antibacterial property of polyethersulfone ultrafiltration hybrid membrane containing halloysite nanotubes loaded with copper ions. *Chemical Engineering Journal* **210**, 298–308 (2012).
63. Yu, Z. *et al*. Effect of functionalized multi-walled carbon nanotubes on the microstructure and performances of PVDF membranes. *RSC Advances* **5**, 75998–76006 (2015).
64. Bottino, A., Camera-Roda, G., Capannelli, G. & Munari, S. The formation of microporous polyvinylidene difluoride membranes by phase separation. *Journal of Membrane Science* **57**, 1–20 (1991).
65. Naik, A. P., Salkar, A. V., Majik, M. S. & Morajkar, P. P. Enhanced photocatalytic degradation of Amaranth dye on mesoporous anatase TiO 2: evidence of C–N, N=N bond cleavage and identification of new intermediates. *Photochemical & Photobiological Sciences* **14**, 1126–1138 (2017).
66. Lee, S.-Y. & Park, S.-J. TiO_2 photocatalyst for water treatment applications. *Journal of Industrial and Engineering Chemistry* **19**, 1761–1769, https://doi.org/10.1016/j.jiec.2013.07.012 (2013).
67. Huo, P. *et al*. Photocatalytic degradation of antibiotics in water using metal ion@ TiO2/HNTs under visible light. *Desalination and Water Treatment* **52**, 6985–6995 (2014).
68. Srivastava, N. & Mukhopadhyay, M. Biosynthesis of SnO_2 nanoparticles using bacterium Erwinia herbicola and their photocatalytic activity for degradation of dyes. *Industrial & Engineering Chemistry Research* **53**, 13971–13979 (2014).
69. Zinadini, S., Zinatizadeh, A. A., Rahimi, M., Vatanpour, V. & Zangeneh, H. Preparation of a novel antifouling mixed matrix PES membrane by embedding graphene oxide nanoplates. *Journal of Membrane Science* **453**, 292–301 (2014).
70. Gupta, V. K. *et al*. Photo-catalytic degradation of toxic dye amaranth on TiO2/UV in aqueous suspensions. *Materials Science and Engineering: C* **32**, 12–17 (2012).
71. Daneshvar, N., Salari, D. & Khataee, A. Photocatalytic degradation of azo dye acid red 14 in water on ZnO as an alternative catalyst to TiO2. *Journal of photochemistry and photobiology A: chemistry* **162**, 317–322 (2004).

72. Chakrabarti, S. & Dutta, B. K. Photocatalytic degradation of model textile dyes in wastewater using ZnO as semiconductor catalyst. *Journal of Hazardous Materials* **112**, 269–278 (2004).
73. Sharma, S., Mukhopadhyay, M. & Murthy, Z. Rate parameter estimation for 4-chlorophenol degradation by UV and organic oxidants. *Journal of Industrial and Engineering Chemistry* **18**, 249–254 (2012).
74. Abdel-Monem, Y. K., Emam, S. M. & Okda, H. M. Solid state thermal decomposition synthesis of CuO nanoparticles from coordinated pyrazolopyridine as novel precursors. *Journal of Materials Science: Materials in Electronics* **28**, 2923–2934 (2017).
75. Zhao, Y., Abdullayev, E., Vasiliev, A. & Lvov, Y. Halloysite nanotubule clay for efficient water purification. *Journal of Colloid and Interface Science* **406**, 121–129 (2013).
76. Mansourpanah, Y., Madaeni, S., Rahimpour, A., Farhadian, A. & Taheri, A. Formation of appropriate sites on nanofiltration membrane surface for binding TiO 2 photo-catalyst: performance, characterization and fouling-resistant capability. *Journal of Membrane Science* **330**, 297–306 (2009).
77. Madaeni, S. & Ghaemi, N. Characterization of self-cleaning RO membranes coated with TiO2 particles under UV irradiation. *Journal of Membrane Science* **303**, 221–233 (2007).
78. Lawless, D., Serpone, N. & Meisel, D. Role of hydroxyl radicals and trapped holes in photocatalysis. A pulse radiolysis study. *The Journal of Physical Chemistry* **95**, 5166–5170, https://doi.org/10.1021/j100166a047 (1991).
79. Houas, A. *et al*. Photocatalytic degradation pathway of methylene blue in water. *Applied Catalysis B: Environmental* **31**, 145–157, https://doi.org/10.1016/S0926-3373(00)00276-9 (2001).
80. Jo, W.-K. & Tayade, R. J. Recent developments in photocatalytic dye degradation upon irradiation with energy-efficient light emitting diodes. *Chinese Journal of Catalysis* **35**, 1781–1792, https://doi.org/10.1016/S1872-2067(14)60205-9 (2014).
81. Jing, H.-P., Wang, C.-C., Zhang, Y.-W., Wang, P. & Li, R. Photocatalytic degradation of methylene blue in ZIF-8. *RSC Advances* **4**, 54454–54462 (2014).
82. Yogi, C. *et al*. Photocatalytic degradation of methylene blue by TiO_2 film and Au particles-TiO_2 composite film. *Thin Solid Films* **516**, 5881–5884 (2008).
83. Orendorz, A., Ziegler, C. & Gnaser, H. Photocatalytic decomposition of methylene blue and 4-chlorophenol on nanocrystalline TiO_2 films under UV illumination: A ToF-SIMS study. *Applied surface science* **255**, 1011–1014 (2008).
84. Rauf, M. A., Meetani, M. A., Khaleel, A. & Ahmed, A. Photocatalytic degradation of Methylene Blue using a mixed catalyst and product analysis by LC/MS. *Chemical Engineering Journal* **157**, 373–378 (2010).
85. Fischer, K. *et al*. Photoactive microfiltration membranes via directed synthesis of TiO_2 nanoparticles on the polymer surface for removal of drugs from water. *Journal of Membrane Science* **478**, 49–57 (2015).
86. Sugimoto, T., Zhou, X. & Muramatsu, A. Synthesis of uniform anatase TiO_2 nanoparticles by gel–sol method: 3. Formation process and size control. *Journal of colloid and interface science* **259**, 43–52 (2003).
87. Hassanien, A. S. & Akl, A. A. Influence of composition on optical and dispersion parameters of thermally evaporated non-crystalline Cd50S50−xSex thin films. *Journal of Alloys and Compounds* **648**, 280–290, https://doi.org/10.1016/j.jallcom.2015.06.231 (2015).
88. Madkour, M., Abdel-Monem, Y. K. & Al Sagheer, F. Controlled synthesis of NiO and Co3O4 nanoparticles from different coordinated precursors: impact of precursor's geometry on the nanoparticles characteristics. *Industrial & Engineering Chemistry Research* **55**, 12733–12741 (2016).
89. Liu, P., Liu, H., Liu, G., Yao, K. & Lv, W. Preparation of TiO_2 nanotubes coated on polyurethane and study of their photocatalytic activity. *Applied surface science* **258**, 9593–9598, https://doi.org/10.1016/j.apsusc.2012.05.154 (2012).
90. You, S.-J., Semblante, G. U., Lu, S.-C., Damodar, R. A. & Wei, T.-C. Evaluation of the antifouling and photocatalytic properties of poly(vinylidene fluoride) plasma-grafted poly(acrylic acid) membrane with self-assembled TiO_2. *Journal of Hazardous Materials* **237-238**, 10–19, https://doi.org/10.1016/j.jhazmat.2012.07.071 (2012).
91. Alem, A., Sarpoolaky, H. & Keshmiri, M. Titania ultrafiltration membrane: Preparation, characterization and photocatalytic activity. *Journal of the European Ceramic Society* **29**, 629–635, https://doi.org/10.1016/j.jeurceramsoc.2008.07.003 (2009).

Acknowledgements

Authors express sincere gratitude to the Sophisticated Analytical Instrument Facility (SAIF), Metallurgical Engineering and Materials Science (MEMS) Indian Institute of Technology Bombay (IIT-B), CSIR-National Chemical Laboratory (CSIR-NCL) Pune and Indian Institute of Technology Gandhi Nagar (IIT-GN) for providing characterization facilities. We are also thankful to the Department of Chemical Engineering, SVNIT, Surat for providing research facilities and MHRD Govt. of India for providing fellowship.

Author Contributions

Mausumi Mukhopadhyay conceptualized the research work and supervised the work done all through with details contribution in discussing and reviewing of the manuscript with technical inputs. Gourav Mishra as part of his PhD research performed all the experiments, characterization, and test, calculation, drawn Figure 13, and data analysis of all results and wrote the manuscript.

Additional Information

Supplementary information accompanies this paper at https://doi.org/10.1038/s41598-019-40775-4.

Competing Interests: The authors declare no competing interests.

Publisher's note: Springer Nature remains neutral with regard to jurisdictional claims in published maps and institutional affiliations.